UNIVERZITA KARLOVA

Přírodovědecká fakulta

Katedra aplikované geoinformatiky a kartografie

Multi-temporal classification of agricultural crops using Sentinel-1

Multitemporální klasifikace zemědělských plodin pomocí dat Sentinel-1

Diplomová práce

Bc. Kamil Kopecký

červenec 2017 vedoucí diplomové práce: RNDr. Přemysl Štych Ph.D.

Prohlášení o autorství

Prohlašuji, že jsem tuto diplmovou práci vypracoval samostatně, pod vedením školitele RNDr. Přemysla Štycha Ph.D., a že jsem uvedl a řádně citoval všechny použité prameny.

Svoluji k zapůjčení této práce pro studijní účely a souhlasím s tím, aby byla řádně vedena v evidenci vypůjčovatelů.

Tato práce ani její podstatná část nebyla předložena k získání jiného nebo stejného akademického titulu.

V Praze dne 31. července 2017 ……………………………….

Kamil Kopecký

Poděkování

Rád bych poděkoval svému vedoucímu práce, RNDr. Přemyslu Štychovi Ph. D, za věnovaný čas, trpělivost a cenné rady. Dále bych chtěl poděkovat Mgr. Adamu Zdobinskému za důležité připomínky a jeho podporu. V neposlední řadě děkuji také rodině a přátelům, kteří mě při zpracování práce a celém průběhu studia podporovali.

Multi-temporal classification of agricultural crops using Sentinel-1

Abstract

This diploma thesis aimed on the exploration of the reflective behavior of individual agricultural crops during the vegetation season. Statistical analysis of agricultural crops was carried out on the basis of multi-temporal SAR C-band Sentinel-1 data. The crop's backscatter was observed during the year 2016. Classification rules were made from detected characteristics. Achieved knowledge was applied and crops separation was done. The result of separation was successful in class Maize. Spring and Winter grains was impossible to distinguish. The possible reasons of poor results are mentioned and further improvements are suggested.

Keywords: SAR, C-Band, crops, object-based classification, SENTINEL-1

Multitemporální klasifikace zemědělských plodin pomocí dat Sentinel-1

Abstrakt

Diplomová práce je zaměřena na zkoumání odrazivých vlastností jednotlivých zemědělských plodin. Statistické veličiny byly zkoumány s využitím multitemporálních radarových dat Sentinel-1 pásma C, poskytovaných Evropskou kosmickou agenturou. Odrazivost vybraných plodin byla pozorována v průběhu roku 2016. Ze zjištěných projevů odrazivosti byla vytvořena klasifikační pravidla. Pomocí zjištěných pravidel byla provedena klasifikace jednotlivých plodin. Úspěšná odlišitelnost byla prokázána pouze u třídy kukuřice. Jarní a ozimé obiloviny nebylo možné spolehlivě rozlišit. Jsou zmíněny možné důvody nepřesností a zároveň navrženy úpravy a metody pro budoucí zlepšení.

Klíčová slova: SAR, C-Band, zemědělské plodiny, objektová klasifikace, Senitnel-1

Contents

LIST OF FIGURES

LIST OF TABLES

LIST OF ABBREVIATIONS

ČHMÚ	Czech Hydrometeorological Office (Český Hydrometeorologický Ústav)
CSA	Canadian Space Agency
DEM	Digital Elevation Model
DoY	Day of Year
ESA	European Space Agency
GCPs	Ground Control Points
GMES	Global Monitoring for Environment and Security
GRD	Ground Range Detected
H	Horizontal
IACS	Integrated Administration and Control System
JAXA	Japan Aerospace Exploration Agency
LPIS	Land Parcel Identification System
NASA	National Aeronautic and Space Administration
RADAR	Radio Detection And Ranging
RMO	Reference mission orbit
ROI	Region Of Interest
SAR	Synthetic Aperture Radar
SRTM	Shuttle Radar Topography Mission
SZIF	State agricultural intervention fund (Státní zemědělský intervenční fond)
V	Vertical
WGS84	World Geodetic System 1984

1 Introduction and thesis objectives

Remote sensing technologies has been providing information of the Earth’s surface for several decades. It is hard to imagine to be without this type of information nowadays. (Jensen, 2000) Data from orbiting satellites bring new insights into global problems solving agenda. It helps to monitor flooded areas, detect geomorphological activities, predict agricultural production and generally provides useful information for landscape management purposes. (Copernicus, 2017)

One of many possibilities of using Earth observation methods is to acquire information about landscape features. For example of vegetation cover, agricultural monitoring, weather forecasting, spatial planning, geomorphological research, fire detection, process of deforestation or desertification. (Copernicus, 2017) Earth observation data are also applicable on water area. Icebergs melting, the quality of water or dry out is observable. The most known example is the dry out of Aral sea, which is very well documented during the years. (ESA-e, 2017) For most of the applications optical data are the main source. They are sufficient for most of the usage but their accessibility could vary. They have limitations in short term investigation as change detection and especially in long term as continuous multi-temporal researches. Remote sensing based on optical sensors is highly dependent on actual atmospheric condition. Sensing with optical is based on reflectance of solar radiation. When the solar energy can not reach the examined feature, it can not be measured. That limits the usage of optical sensors only on daytime and days without clouds. (Grandoni, 2013) In the area of central Europe there could be days without clouds. The situation is problematic in tropical areas. There could be constant cloud coverage whole year. The optical sensing over those parts is useless.

The potential alternative is RADAR – SAR technology. The main advantage is an independence of solar radiation. Radar is an active emitter. Its radiation penetrate the atmospheric features and allows sensing the surface even in cloudy days. (Grandoni, 2013) That is appreciated the most in the tropical and monsoon areas. Even over the areas without cloud cover, there is an usage for this type of data. The continual sensing provides possibility to observe seasonal development of selected crops, which is important for related activities. Thanks to those information, precise agriculture could be improved, climate variation or changes according to vegetation cycles could be observed, the wealth of crops and estimation of yield could be done. (Copernicus, 2017)

Science is currently seeking to streamline agricultural practices. Whether the goal are sustainable land or maximum yields, Earth observation is appropriate to use and the classification of crops is one of the part.

One of the goal of the thesis is the research of literature and academic works about classification of agricultural areas using RADAR data. The research aims on selected crops that are relevant to our environment. Relevant parts of the SAR data will be discussed, primarily about their geometry and acquisition. The steps of data processing and its options will be observed. Based on those information the SAR data will be processed.

Other important goal of the thesis is exploration of characteristics of selected crops in SAR C-band. In this thesis it is aimed on the exploitation of multi-temporality of those data. Statistical characteristics of backscattered energy will be observed. The proper explanation of those characteristics connected to backscatter theory of C-band SAR data will be presented

Last objective of the thesis is selecting and defining the best periods and best parameters to distinguish individual crops. According to the research, the most suitable classification approach is used and selected crops are classified.

In the last part the results will be presented in statistical and cartography form. Problems that could appear are discussed and potential of further research will be outlined.

2 SAR application in agriculture

From the studies about land cover classification that has been realized is known that SAR C-band is suitable. Ferazzoli (2001) confirms C and L band appropriate to use in agriculture and mention the possibilities of multi-temporal advantages of SAR data.

Del Frate et al. (2003) aimed on classification agriculture crops with combination of space born SAR (ERS) and air born SAR (AirSAR). In their study the neural net and maximum likelihood method was tested. The results of classification were successful, up to 98 %. As the best approach the per-field classification was selected. Thanks to available dataset of agricultural parcels were the boarders are known this method could be used. There is also mentioned the thought about real time classification. This possibility is supported by the results when winter wheat was successfully classified in the beginning of March.

The importance and suitability of vector layer of crop field confirms Tavakkoli et al. (2012). In their study different approaches and methods of classifications were tested. As the best classification the maximum likelihood was pointed. The benefit of speckle filtering is mentioned. As the best speckle filter the Lee 7x7 was signed.

Skrivera et al. (2012) focused on the multi-temporality and polarization in their study. It was affirmed that dual polarization can possibly provide better information capacity to process better classification. Higher temporality and more of the images during the season improves the accuracy (even for single or dual polarization). The benefits of multi-temporality are mentioned also in Tavakkoli (2012) and Del Frate (2003).

According to Blaes (2002), it his helpful to have information about boarders of single fields. He agrees with positive impact of higher temporal resolution. To eliminate the effect of soil moisture, he suggests to remove images captured in the time after rain. That should improve the accuracy of classification.

There is also an approach how to distinguish crops, where beside of intensity, the phase is used. Moeremense and Dautrebandeho (1998) used images of one day difference. Thanks to that the height of the vegetation could be measured. It is also mentioned that with the coherence, there is a possibility to detect bare surface. That information could leads to separation of single crops. Klenke and Hochschild (1999) also aimed on usage of coherence. In their article it is said, that at winter crops have lower coherence in March and April. For the individual type of crops there was selected optimal period of observation. Winter crops 110. to 220. day of the year (20.4.-8.8.). Spring crops 130-180 DoY (10.5.-29.6). (Satalino, 2014)

External influences on the backscatter in SAR was examined by Saich and Borgeaud (2000). By freezing of soil it lead to significant reduction of backscatter reflection. On the other hand, when the temperature raised, the ice melted and the backscattered intensity got higher. The reflectivity of soil is higher with presence of water. The reflection is also affected by drops on vegetation canopy.

Crop development is described by Skriver et al. (1999). On the field were spring wheat is located, there is a bare soil in May. They are growing during the June and in July. Winter wheat starts the vegetation cycle first. In July they are already full grown and in the phase of ripening. In their study they found out that using of combination of images from May and July in C-band it could get better result than using them separately. Which confimrs the benefit of multi-temporality.

There is problematic part when winter and spring wheats have to be distinguish. The classification has been done on the images of VV polarisation from May to July. Maximum Likelihood was used. The results were sufficient but the authors say, that better results could be achieved by field segmentation and speckle filtering (Schmulliuse, Nithack (1995). As an advantage in multi-temporal approach Skriver (2012) sees the presence of June image. On the other hand the April image is found as redundant. He says that the minimum errors are achievable using 4 images.

Oleggini (2008) says that the HH polarisation is corresponding with the reflectance during the planting. For the agriculture observation is characteristic the variability of intensity values during the year. The growth of values during the ploughing is caused by roughness of soil after that. The surface get flat naturally and the intensity gets lower. When the crops start to grow they make the surface rough and so the values get higher. After the crops are fully grown and are in the phase of ripening, the surface get dry and the values of intensity backscatter get low. The last significant moment is at the end after harvest, when there is a higher roughness of the surface. In Figure 1 there is a graph of optical and radar data. It is visualised with the vegetation stages during the year.

Figure 1: Comparation of SAR backscatter with vegetative stages

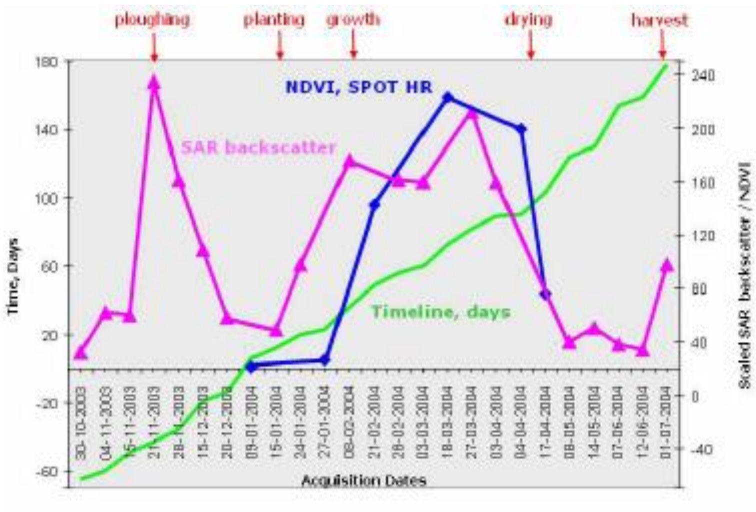

Source: (Oleggini, 2008)

Pixel based approach was tested in the study of Mather and Tso (1999). There was seven images from April to September of C-band ERS-1. The supervised classification was investigated. They vectorize the single fields and then got the statistics of it. The accuracy assessment was not that high as they expected. They suggest to include optical images and consider object based approach.

There was a study in central Germany. The classes for classification was selected according to those that were present there. Water bodies, urban area, forests, agriculture area, grassland. Thiel et al. (2009) used the ERS-2 data. One of the aim of the study was to approve the potential of the Sentinel mission which is also C-band. Three polarization were used, HH, VV and HV. Minimum, maximum and the mean values of intensity from all 27 images. The best classification results were achieved with mean values.

3 Introduction to SAR

3.1 History of SAR

Imaging radar has its first significant impact in the remote sensing in 1978. At that year the SEASAT satellite for ocean and ocean ice observation was launched. For those times in sufficient spatial resolution 25 m. (Čapek, 1988) On board of this satellite, the technology of synthetic aperture was first used. Although the mission took just 105 days, the benefit of such instrument was proven. It stimulated further development in this area. Other institution beside NASA tried to develop their own devices and so SEASAT was followed by ERS-1, 2, (ESA), JERS-1 (JAXA) or RADARSAT- 1 (CSA).

The period of space born full polarized radars started in 1994, when SIR-C was launched. Thanks to that the first full polarized images of the Earth was taken followed by ALOS, TerraSAR-X, RADARSAT-2 and now Sentinel-1. (Lee, Pottier, 2009)

3.2 SAR

Synthetic Aperture Radars were developed as a means of overcoming the limitations of real aperture radars. These systems achieve good azimuth resolution that is independent of the slant range to the target. Use small antennae and relatively long wavelengths. (ESA, 2017) Radar with synthetic aperture is an active sensing device. Active sensors, provide their own energy source for illumination. The sensor emits radiation which is directed toward the target. The radiation reflected from that target is detected and measured by the sensor. Advantages for active sensors include the ability to obtain measurements anytime, regardless of the time of day or season. Active sensors can be used for examining wavelengths that are not sufficiently provided by the sun, such as microwaves. (NRCANa, 2017) List classes of microwave spectrum wavelengths and their designations is in Tab. 1. The device is set on board flying platforms. Planes (air-born) and devices attached to satellites (space-born) are used. Synthetic aperture is produced by using the forward motion of the radar. As it passes the scatterer, many pulses are reflected in sequence. It is important to note that some details of the structure of the echoes produced by a given target change during the time the radar passes by. This change is explained also by the Doppler effect which among others is used to focus the signals in the azimuth processor. (ESA, 2017)

Table 1: An overview of the bands and the dimensions of their wavelengths

Band	Wavelengths
P-band	107-77 cm
UHF	100-30 cm
L-band	30-15 cm
S-band	15-7,5 cm
C-band	7,5-3,75 cm
X-band	3,75-2,40 cm
Ku-band	2,40-1,67 cm
K-band	1,67-1,18 cm
Ka-band	1,18-0,75 cm

Source: Cambel (1987)

3.3 Geometry of SAR

The SAR devices consist of a transmitter, an antenna, a receiver and a system that records and processes the data. The imaging geometry of SAR is different from instruments dealing with optical data. The essentials are described in Figure. 2

Figure 2: Viewing geometry and spatial resolution

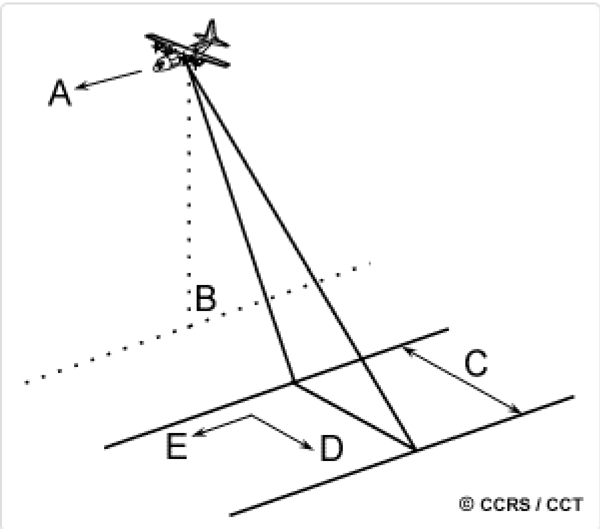

Source: NRCAN-b (2017)

The direction represented by letter A is the flight direction. Letter B is a place called nadir. It is always located directly beneath the instrument. Area of the surface, where data are collected is called swath (C). Data of Sentinel-1 in IW mode have the swath width 250 km. D, range, is an across-track dimension, perpendicular to the direction of the motion. Azimuth dimension E is the direction of the flight. (NRCAN-b, 2017) (Lee, Pottier, 2009)

The incidence angle is the angle between the radar beam and ground surface which increases, moving across the swath from near to far range. The look angle is the angle at which the radar "looks" at the surface. In the near range, the viewing geometry may be referred to as being steep, relative to the far range, where the viewing geometry is shallow. At all ranges the radar antenna measures the radial line of sight distance between the radar and each target on the surface. This is the slant range distance. The ground range distance is the true horizontal distance along the ground. It is corresponding to each point measured in slant range. (NRCAN-a, 2017)

3.3.1 Distortions

Since the radar measures the distances in slant-range, a near range area of the image appear compressed according to the far range. This distortions are corrected by converting to ground-range display. (Parker, 2012)

Geometric distortions are also crucial chapter in understanding of radar imaging. Due to the relief displacement, three typical distortions could appear in the image.

Foreshortening

Effect of foreshortening is present in the image if the terrain ad its slope is inclined toward the radar beam. The distances in a slant-range image are shorten. It is caused by different elevation. The point on the higher ground appears to be closer to the radar and is recorded closer to the lower elevated points in the direction towards the radar. The areas affected by foreshortening appears steeper than they are. Foreshortening is caused by object height, the higher the point the bigger the effect of foreshortening. The size of incident angle. The smaller the incident angle the bigger the foreshortening. And last influence is the location in the across-track range. Areas in near-range are foreshortened more than those in far-range. (Jensen, 2000), (Parker, 2012) Creation of the distortion is shown in Figure 3.

Figure 3: Foreshortening

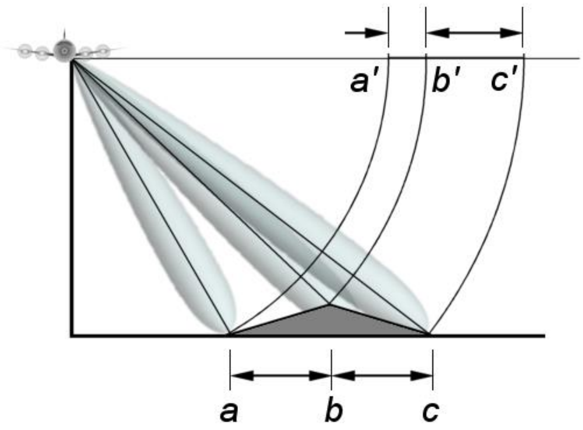

Source: Radar Basics (2017)

Layover

Image layover is an extreme case of foreshortening effect. It happens when there is high difference in elevation between the top and the base of the mountains. The signal is back scattered from the summit earlier than from the base. The summit in the slant-range image lays over the base. This distortion can not be fixed with terrain correction. (Jensen, 2000), (Parker, 2012) Layover distortion is shown in Figure 4.

Figure 4: Layover

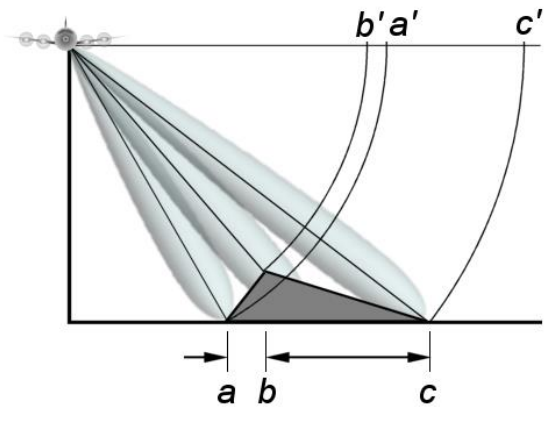

Source: Radar Basics (2017)

Shadow

Presence of shadow in the image signify the geomorphology and terrain situation in the area. The mountains, building and other elevated features could be distinguished. The position of the shadow also says about look direction of the radar. The shadow is made when the backslope is greater than depression angle. The size or even presence of shadow vary in across-track. Shadow that is in far-range does not have to be in near-range. (Jensen, 2000), (NRCAN, 2017), (Parker, 2012) An illustration of the shadow is shown in Figure 5.

Figure 5: Shadow creation

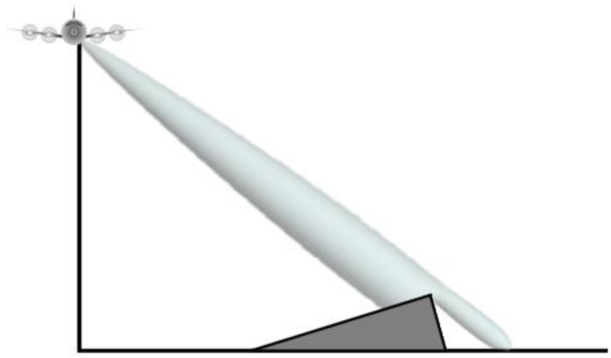

Source: Radar Basics (2017)

3.3.2 Spatial resolution

To achieve high resolution in range dimension, very short pulses have to be emitted. Trying to fulfil this condition and in the same time obtain a sufficient signal-to-noise ratio, it is necessary to generate pulses with high energy. Otherwise the reflected signal will not be detected. Because of this, the compression technique of longer pulses with high energy is used. It is called chirp. Applying filter, the results are comparable with signal of very short impulses. Ground range resolution varies nonlinearly across the whole swath according to actual incidence angle. (Lee, Pottier, 2009) Equation of range resolution according to Sarti (2009) is following:

$$r = \frac{c}{2 \times Br \times \sin\theta} \tag{1}$$

where *Br* is bandwidth frequency of pulse, *c* is speed of light and θ is look angle

Resolution in azimuth depends on the wavelength and the size of the antenna. With shorter wavelengths better resolution could be obtained. To reach high resolution with relatively short antennas the synthetic aperture is used. Azimuth resolution is independent of a range. (Johannessen et al., 2013) The rule is that azimuth resolution is equal to a size of half of the antenna. (Jensen, 2000), (Sarti, 2009) Azimuth resolution is calculated as follows:

$$a = \frac{L}{2} \tag{2}$$

where *L* is length of antenna

3.4 Roughness

Without the contribution of water inside the soil, brightness is an effect of roughness. Farr G.T. (1993) describes roughness as a function of wavelength of pulse and its incidence angle. He divides roughness into three classes. Smooth, Intermediate and Rough. Equations of classes are following. Calculation for our data was performed.

Smooth	$h \leqq \frac{\lambda}{25 \cdot \cos\theta}$	$h \leqq \frac{5{,}55}{25 \cdot \cos 37{,}5}$	$h \leqq 0{,}279\ cm$	(3)
Intermediate	$h = \frac{\lambda}{8 \cdot \cos\theta}$	$h = \frac{5{,}55}{8 \cdot \cos 37{,}5}$	$h = 0{,}874\ cm$	(4)
Rough	$h \geqq \frac{\lambda}{4{,}4 \cdot \cos\theta}$	$h \geqq \frac{5{,}55}{4{,}4 \cdot \cos 37{,}5}$	$h \geqq 1{,}589\ cm$	(5)

h represents height of difference
λ represents wavelength of pulses which is in our case 5,55 cm
θ represents incidence angle which for our data vary between 29,1° and 46°

3.5 Soil moisture

Different types of terrains and soils conduct electricity better than others. The ability of that describes complex dielectric constant. Dry surface features without presence of water have dielectric constants from 3 to 8. Water on its own has up to 80. The amount of moisture in soil or vegetation have effect on amount of backscattered energy. The amount of moisture also affect the depth of penetration. If there is a lot of moisture in the top layers, the energy reach only the top and then backscatter. If the soil is dry the energy signal penetrates according to its wavelength. The longer it is the greater the penetration is. (Jensen, 2000)

3.6 Polarization backscattering

Although the polarized electromagnetic energy is used only in recent past, the first discoveries could be dated to the ancient times. The Vikings were using crystals and its ability to refract light for navigation. The modern discovery of light polarization is associated with Erasmus Bartolinus and Christaan Huygens. Electromagnetic radiation is a combined out of two parts. Electric and magnetic vector. They are perpendicular to each other and to the direction of propagation. But those vectors act unpredictably. Polarized radiation has defined the direction of those vectors. There is linear, circular and elliptical polarization. (Lee, Pottier, 2009)

Like polarization backscatter (HH, VV) signify single reflection from canopy components as leaves, branches, trunk. The returns are in general very strong and in the image look bright. It is called canopy scattering. If the energy is scattered multiple times, the energy become depolarized. Those backscatterers could be distinguished in VH and HV. There are some other observations that approximate vegetation interpretation. Vertically polarized energy is attenuated by vertically oriented canopy features. On the other hand horizontally polarized energy more backscattered by horizontal planes. The brighter backscatter of like polarized energy HH and VV, the bigger the contribution of surface scattering. Higher cross polarized backscatter HV and VH, the higher the volume scattering. (Jensen, 2000), (Parker, 2012)

3.7 Speckle noise

Speckle noise is present in all coherent imaging systems as laser and SAR imagery. Radar waves interfere producing light and dark pixels known as speckle noise. The origin of the noise is assigned to unsystematic interference between the coherent returns of the signal from the scatterers on the surface. Speckle noise is usually understood as an undesirable effect. That is why speckle filters were developed. (Mansourpor, 2006), (Gagnon, 1997)

There are two groups of speckle filtering techniques. Multi-look integration and post-image formation methods. The first method works in a way of averaging independent images called looks into one. In case of Sentinel-1 data, the process of multi-look filtering is already done by ESA. The second group of filtering techniques consists of well-known common used standard filters as Medain, Kuan, Lee, Frost and many others, called spatial filters.

Speckle filtering consists of moving kernel above all pixels. It calculates over every pixel inside the kernel and replaces the central pixel with calculated value. Applying these types of filters a smoothing effect is achieved while speckle noise is reduced.

Lee Filter

Lee filter uses the statistical distribution of the values within the moving kernel to estimate the value of the pixel of interest. It is based on the assumption that the mean and variance of the pixel of interest is equal to the local mean and variance of pixels inside the moving kernel. Lee filter is meant to minimize difference between the filtered result and the true intensities. (Gagnon, Jouan, 1997) The equation for Lee filter according to Mansourpor (2016)is:

$$DNout = [Mean] + K[DNin - Mean] \tag{6}$$

where $K = \frac{Var\ (x)}{[Mean]^2 \times \sigma^2 + Var\ (x)}$

and

$$Var\ (x) = \frac{[Variance\ within\ window] + [Variance\ within\ window]^2}{[Sigma]^2 + 1} - [Mean\ within\ window]^2$$

It was derived from the minimum square error criteria introducing the local statistics in it. It was believed that it will reduce the speckle and preserve the edges. (Huang, 1996)

3.8 SAR image interpretation

The way, how to correctly interpret the SAR image is not that clear task, compared to optical images. To understand reasons of backscattering the knowledge of ground conditions is needed. There are some general rules that help to understand. (NASA, 1987)

Dark areas in the SAR images represent surfaces such as roads, runways and especially calm water areas. From these types of flat surfaces, most of the radar pulses are reflected away of transmitter. That leads to having low values of backscattering coefficient. The reflection is similar to the mirror reflectivity where the angle of reflection is equal to angle of incidence. There are some interesting facts about appearance of water in SAR images. Calm waters appears dark, the rough water surface appears relatively bright. The waves backscatter signal to variety of direction which leads to higher probability that more of it will reach the receiver. Bright areas represent rough surfaces. That is the case of the ships, buildings or most of the man-made features in general. The very bright targets are caused by double bounce or corner reflector. This characteristic makes possible to detect ships, whose are brighter even than rough water surfaces. Also the oil films that smooth the surface are detectable. (Parker, 2012)

The interpretation of soil and vegetated areas is more complicated. As was said before, the main characteristic is roughness or smoothness. Rough soil areas have higher backscatter reflection than smooth areas. Soil reflectivity does not depend only on roughness. The important part is also the presence of water, moisture. Higher soil moisture leads to higher backscatter. It is important to say, that the roughness and smoothness are relative to the wavelength of the pulses. In the image of L-band the 5-10 cm fluctuation of the surface is shown as dark area. In X-band image, which has a short wavelength this fluctuation would appear bright. (CRISP, 2017)The list of bands is shown in Tab.1

Crops in C-band

Theoretically the sigma nought values at C-band should be affected by following elements. In the beginning of the season, the signal interacts only with the bare soil. The values are affected by the soil moisture or its roughness. Since there is only single backscatter - VV band is appropriate to use. In this part of the season the fields are flat and without any crops. That means that the reflectivity should be lower. When the plants are visible on the surface, the signal starts to interact with the plants. The backscatter is higher. In combination with rain even higher. Period of growth of crops is visible as increase of reflectivity in VH band. VH band represents the volume scattering caused by vegetation. The phase of ripening, when the moisture of canopy decreases, sigma nought values decrease. When the crop is harvested the signal of VH has nothing to interact with, so the values are low. On the other hand the surface remains flat and bare so the single backscattered energy increase could be detected in VV band. (Jensen, 2000)

4 Crop types

4.1 Winter cereals

The group of winter cereals or grains is made out of crops with specific characteristics. It could be barley, rye, wheat. These crops are breeded to special condition. They are sown in autumn (15.9. – 20.10.) and germinate before winter comes. They could grow even during the mild winter. Normally they just preserve until spring. Then continue their vegetation cycle until harvest, which is in summer. Usually at the end of July. Harvest period can start earlier than for spring grains. The motivation for growing winter types of grains is to distribute agricultural works. The advantage of growing winter cereals is also higher yields. (Lagerhouse, 2017)

4.2 Spring cereals

Group of spring grains contains predominantly the same types of crops that were mentioned previously. The difference is that they are adapted to different vegetation cycle. They are planted in early spring and mature in second half of summer. Compare to winter grains they require more irrigation and yield is lower. Optimal period of sowing is between second half of March and beginning of April. (Lagerhouse, 2017)

4.3 Maize

Sowing of maize seeds takes place in later spring when the minimum temperatures are around 10°C. the period of sowing maize in Czechia is in late April until the half of May. The harvesting period could vary according to use of the maize. In Czechia there is usually maize for fodder, that is harvesting in early autumn in September. (APIC, 2017)

5 Object based classification

Classification is a process of automatic evaluation of the image. According to the specific rules, every pixel is included in one of the classes. Those rules are developed according to spectral, temporal, spatial and polarimetric resolutions. (Halounová, 2004)

Object based classification always starts with a segmentation of the image. The image is cut into single blocks with similar characteristics. The segmentation can be done by splitting image into regular or varying squares or by merging the neighboring pixels with similar values. After a segmentation, the rules have to be set. According to those rules the single features can be distinguished in the image. (SlideShare, 2010)

The advantages over a pixel-based classification is that object-based approach minimize the salt and pepper effect that usually affects pixel based approach. Other features that help to distinguish classes as spatial, textural and contextual properties could be derived to improve the classification accuracy. (Liu, Xia, 2010) This method is chose also according to the conclusion of Mather and Tso (1999) and (Schmulliuse, Nithack, 1995), as mentioned before.

5.1 Rule-based classification

Every class is defined by classification rules. Segments are classified into the classes based on the rules defined by user. The rules could have one or more attributes. The range of values for every attribute has to be set. Those attributes and rules can be combined together. Weight of selected rule if necessary or threshold for segregation of unclassified segments could be set. In Figure 6 there is an example that illustrate how classification rules could be used. (Exelis VIS-a, 2017)

Figure 6: Rules setup

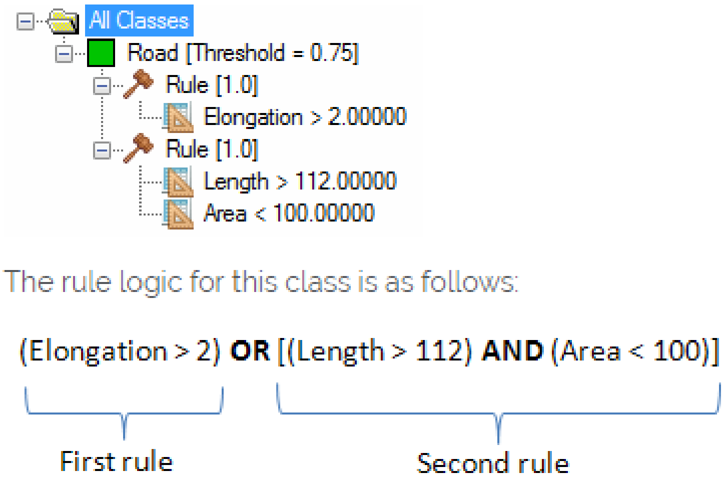

Source: Exelis VIS-a (2017)

6 Data and area of interest

This chapter introduces the area in which the areas under investigation are located. Their location is shown here. Description and visualisation of the data relevant to achievement of stated goals is presented.

6.1 The area of analysis

The area upon it was decided to observe the behaviour of crops is located in Czechia. This is because the crops that were chosen for observing are in abundance present there. The requirement of the ground truth data was also one of the conditions. It was recommended to work in the area where information is available and for that reason the area in east part of Czechia was chosen. The area is located in the area of Olomoucký. Zlínský and Moravskoslezský region. The area was chosen with intention to have all selected fields in one scene. Thanks to that the time of processing was minimalized.

The area is located in the central Europe, where the continental and coastal climates neighbour. Four seasons change during the year and the vegetative cycle is from March/April until September. (EAGRI, 2011) Precipitation is on the medium level of 637 mm per year. The most intense rainfalls appears in summer months. The average temperature of the year 2016 was 8,7 °C. June, July and August as the most warm months, had an average temperature between 17 and 18 °C. (CHMI, 2017)

6.2 Data

6.2.1 Satellite imagery

The Sentinel-1 data that are used in this thesis are acquired by ESA, through the programme Copernicus. There are other options to select. But according to our research and needs of this study Sentinel-1 data meet the requirements.

They were chosen because they are up-to-date. The mission started in recent past so the instrument produces high quality data. For study it was necessary to have continuous dataset that was collected during the whole vegetation season. In the 2016 there is only one image missing (June 25) because of a defect of instrument. Sentinel mission provides data with 12 days period between acquisitions of the same area. This multi-temporality is one of the biggest advantage that is used in many different fields. (Copernicus, 2017) In Table 2. there is a list of acquisition dates and orbits of used images.

The sensor is able to collect data in different polarisation, VH and VV with spatial resolution 10x10 m. (ESA-c, 2017) There are other devices, that can achieve better resolution as TerraSAR- X or COSMO-SkyMed 1 but for purpose aimed on agriculture in selected area, the capacity of Sentinel -1 data are sufficient. Sentinel-1 data are public, for free and easy and fast available.

Sentinel-1 operates in C-band at wavelength λ = 5,55 cm. In Interferometric wide swath the angle of incidence vary between 29,1° and 46°. (ESA-c, 2017)

Sentinel data products are distributed using a SENTINEL-specific variation of the Standard Archive Format for Europe (SAFE) format specification. The SAFE format has been designed to act as a common format for archiving and conveying data within ESA Earth Observation archiving facilities. SAFE was recommended for the harmonisation of the GMES missions by the GMES Product Harmonisation Study. (ESA-d, 2017)

The scene that was chosen has relative orbit number 73. The direction of overpass while acquisition of image is ascending. The image covers the area of eastern part of Czechia in the rectangle bounded with geographic coordinates: [14.684813 50.057888], [18.348606 50.468655], [18.705997 48.972675], [15.151957 48.563416]. This orbit was chosen as a compromise of requirements of the insitu data. Location of scene is shown in Figure 7.

Figure 7: Location of selected scene

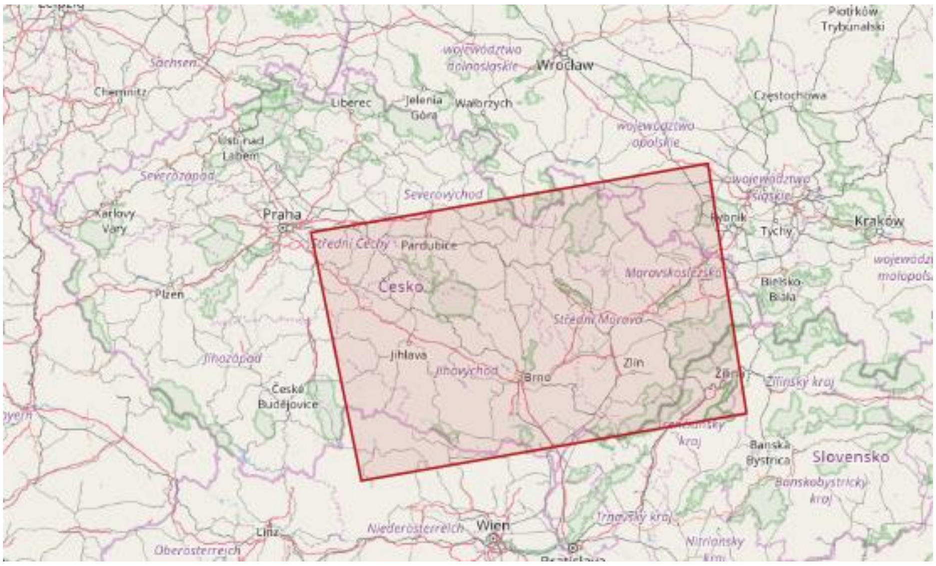

Source: own screenshot from Copernicus Open Access Hub

Table 2: Used data

Date	Orbit number	Date	Orbit number
2.4.2016	10645	19.7.2016	12220
14.4.2016	10820	31.7.2016	12395
26.4.2016	10995	12.8.2016	12570
8.5.2016	11170	24.8.2016	12745
20.5.2016	11345	5.9.2016	12920
1.6.2016	11520	17.9.2016	13095
13.6.2016	11695	29.9.2016	13270
		11.10.2016	13445
7.7.2016	12045	23.10.2016	13620

Source: (Copernicus Open Access Hub)

In the addition it also should be said that GRD products that are downloaded, have been already multi-looked and set to ground range using an Earth ellipsoid model WGS84.

6.2.2 Ground-truth data

Ground-truth data that are used in the thesis were collected by private company GISAT s.r.o. The data are sorted in ESRI shapefile.

This shapefile contains attributes that describe the type of the crop. As it was said in the previous section, the study is aimed on winter and spring grains and maize. This information was collected in three phases, on the edge of March/April, May/June and October. The multiplicity of field surveys is important in our case. If there will be only one survey some information could be missing. For example in spring not all crops are already grown so it is better to realize another observation in latter month in the summer. There were 102 fields provided by GISAT s.r.o.,. In Figure 8, there is a geographical location of mentioned data.

Figure 8: Ground truth data overview

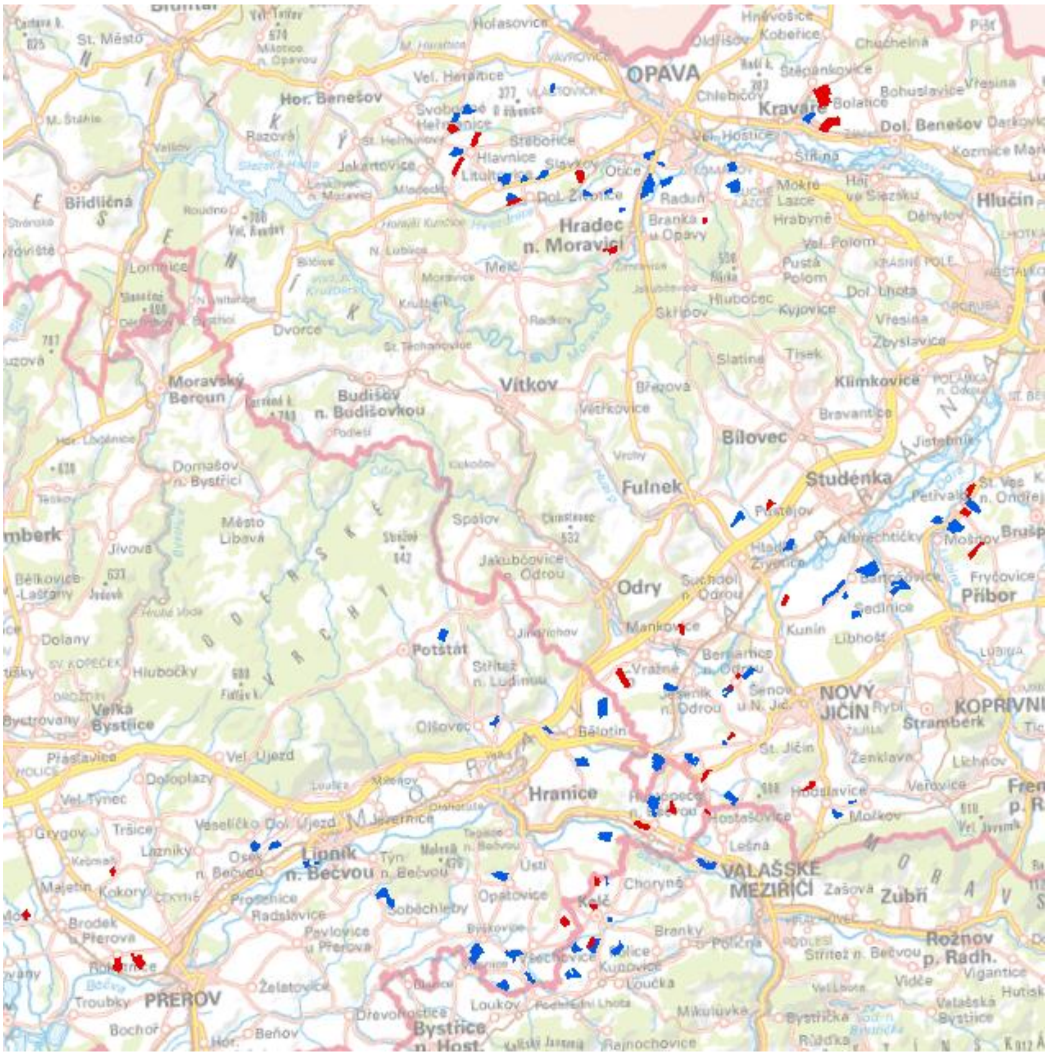

Source: ČÚZK (2017), GISAT (2017)

Dataset was divided into training and validation polygons. Training polygons are red and validation polygons are blue. The selection was made with the intention of dividing the dataset so that twice more polygons are in the validation set. Data and their dimensions are in Table 3.

Table 3: Ground truth data characteristics

Category	Training polygons [km^2]	number of training polygons	Validation polygons [km2]	number of training polygons	mean slope [°]
Maize	2,044	12	4,118	23	2,77
Spring grain	3,056	10	4,358	25	2,66
Winter grain	1,355	10	5,144	22	2,66

Source: GISAT (2017), LPIS (2017)

6.2.3 LPIS

Land Parcel Identification System is a database in which all the agricultural area of the state is stored. LPIS is the key component of the Integrated Administration and Control System (IACS) for area based subsidies. It is the modern supporting tool in the form of a spatial register used within an IACS environment. It helps the farmer who intends to apply for aid under any of the area-related aid schemes to identify any agricultural parcels intended to be listed in his annual declaration for EU aid. (ARPA, 2017) Administrator of the system in Czechia is the Ministry of Agriculture and SZIF. Data are freely available in shp format.

6.2.4 DEM

In the SAR image processing the DEM is needed. It could be used for masking out the shadow areas or as in the case of this thesis the DEM was used for terrain corrections. Terrain corrections are intended to compensate distortions so that the geometric representation of the image will be as close as possible to the real situation. (NEST, 2017) For this intention the SRTM DEM was used.

Shuttle Radar Topography Mission was the mission of National Aeronautics and Space Administration NASA and National Geospatial-Intelligence Agency NGA. The mission focused on acquisition global coverage of elevation data to create global elevation model of the planet. The instrument was carried out on the orbit by space shuttle

Endeavour on 11. 2. 2000. The mission took 11 days. The shuttle made 176 overpasses and the data of 80 % of the planet's surface were collected in between 60° north and 56°south latitude. Two versions were generated afterwards. Nowadays both of them, with 30 m and 90 m pixel spacing are freely available. Agricultural parcels in Czechia are large so that the 30 m resolution was accepted as sufficient. (USGS, 2015)

6.2.5 Meteorological data

Due to the findings of Blaes (2002) and Saich and Borgeaud (2000) attention was paid to meteorological conditions. They say that it is advisable not to use images taken after the rain to eliminate the effect of soil moisture.

ČHMÚ stores meteorological data about precipitation and temperature in each day. The dataset contains data, since 1961. Data is collected in 10 stations. It is provided in excel files. Stations that are closest to the area of our interest were chose. Brno Tuřany and Mošnov. Lysá hora is also nearby but is located in the mountains, where the conditions are different. Because of this, data was not used. Overview map is in Fig. 9. The graph of precipitation measured in selected stations is in Fig. 10. Data that are the basis of the graph are stored in Tables 4 and 5. In the brackets are data from the previous day. These days are displayed as bars.

Figure 9: Map overview of meteorological stations

Source: CHMI (2017)

Figure 10: Graph of precipitation

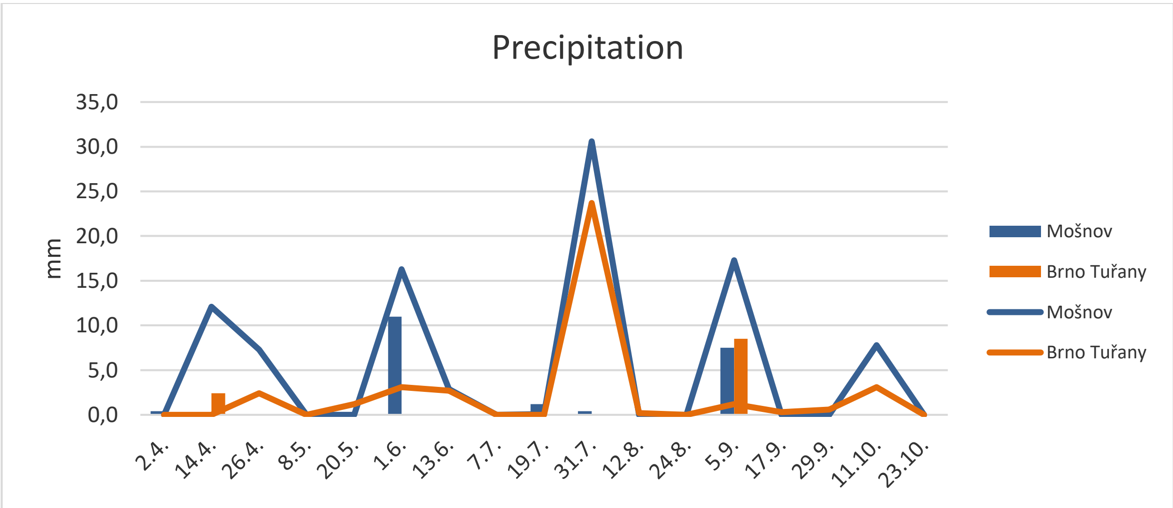

Source: CHMI (2017)

Table 4: Precipitation at station Mošnov

Date	mm	Date	mm
2.4.2016	0 (0,4)	19.7.2016	0,1 (1,2)
14.4.2016	12,1 (0,0)	31.7.2016	30,6 (0,4)
26.4.2016	7,3 (0,1)	12.8.2016	0 (0,0)
8.5.2016	0 (0,0)	24.8.2016	0 (0,0)
20.5.2016	0 (0,0)	5.9.2016	17,3 (7,5)
1.6.2016	16,3 (11,0)	17.9.2016	0 (0)
13.6.2016	2,0 (0,0)	29.9.2016	0 (0,0)
		11.10.2016	7,8 (0,0)
7.7.2016	0 (0,0)	23.10.2016	0 (0,0)

Source: CHMI (2017)

Table 5: Precipitation at station Tuřany

Date	mm	Date	mm
2.4.2016	0 (0)	19.7.2016	0 (0)
14.4.2016	0 (2,4)	31.7.2016	23,7 (0)
26.4.2016	2,4 (0)	12.8.2016	0,1 (0)
8.5.2016	0 (0)	24.8.2016	0 (0)
20.5.2016	1,2 (0)	5.9.2016	1,2 (8,5)
1.6.2016	3,1 (0)	17.9.2016	0,3 (0)
13.6.2016	2,0 (0)	29.9.2016	0,6 (0)
		11.10.2016	3,1 (0)
7.7.2016	0 (0)	23.10.2016	0 (0)

Source: CHMI (2017)

7 Multi-temporal analysis

7.1 Data processing

To get values that represent the actual reflective properties of the surface, several steps are needed to be done. The Level-1 products already went through the process of multi-looking and are georeferenced to ground range. These “raw“ images need to be processed through common steps as radiometric correction, speckle filtering and terrain correction. (ESA,1993).For processing imagery data, SNAP software is used. Because data are provided by a developer of that software, this program was assumed as best choice to use.

The chain starts connecting images with information about the orbit of the instrument to get precise results. There was a mission that was supposed to select and measure the Reference Mission Orbit (RMO). The orbit was reached in August 2014. All the satellites that are now in service are kept in Orbital Tube with radius of 50 (rms). (ESA-b, 2017) Using the function Apply Orbit File, the information of the instrument’s location, according to RMO is calculated. The orbit file provides accurate satellite position and velocity information. Based on this information, the orbit state vectors in metadata of the product are updated. Precise orbits are produced a few weeks after acquisition. With precise orbit file, possible inaccuracies in the image could be fixed. (ESA-b, 2017)

The important step is Calibration. It always has to be in the beginning. (Veci, 2016) Calibration transform the values that the instrument received into the sigma nought values. Those values represent the real reflective properties of the surface. Calibration is the process of quantitatively defining the system response to known controlled signal inputs. Calibrated SAR images are essential to quantitative use of SAR data. A calibration vector is included as an annotation in the product allowing simple conversion of image intensity values into sigma nought values. (ESA, 2013)

In this moment the image with real reflectivity information is prepared. The problem with speckle noise has to be solved. Some scientists support speckle filtering as a necessary part of the chain. In their point of view, the speckle noise reduces quality of the data and to get the proper values, filtering is indispensable. The others understand the process of speckle filtering as the loss of real information that devaluate the results. (Mouratidis, 2017) According to the research that has been made, it was concluded to apply speckle filters to remove the speckle noise. Lee 7x7 speckle filter was selected. As has been said, some details of the original data are modified, but should not have influence on the result. Tavakkoli et al. (2012)

Geometric Range-Doppler Terrain Correction is following part in the chain of processing. Due to topographical variations of a scene and the tilt of the satellite sensor, distances can be distorted in the SAR images. Image data that are not directly at the sensor's nadir location have some distortion. Terrain corrections are intended to compensate for these distortions so that the geometric representation of the image will be as close as possible to the real world. (NEST, 2017) To proceed the terrain correction the DEM is needed. For Sentinel-1 application there is a possibility to download the SRTM immediately from the online storage. Bilinear interpolation was chose. Bilinear resampling is a good compromise between processing time and complex generation of the new raster. (Braun, 2017)

The output of these settings is geocoded, terrain corrected image of sigma nought values in WGS84 N33 projection.

For further work the sigma nought images of both VV and VH polarisation were exported into GeoTIFF format, to be possible to work in QGIS. The export could not be done easily since the whole scene is 250 km wide and the image has a big amount of data. The sub-scene of the specific area, where the agricultural fields are located, was exported.

In QGIS the raster and the vector layer of agricultural fields were visualised. Because the satellite images are stored in WGS84 N33 projection, vectors were transformed from S – JTSK to WGS84 N33. The spatial resolution of raster is 10 x 10 m. There were some cases, when some scatterers that were not part of the field, affected the pixels that were inside the polygon. It was clear that those pixels should not enter the analysis. Due to this situation the size of polygons was reduced by 40 m along the border. That prevented unwanted effects to participate on the results. The minimum number of pixels so that the value was representative was set to 300. Ten spring grains polygons, ten winter grains polygons and twelve maize polygons came into the statistical analysis. Polygons that appeared homogeneous were selected.

Zonal statistics were computed in selected polygons from each class. From statistics as Standard deviation, Minimum, Maximum, Minority, Majority, Median, Range and Mean, only the last statistical characteristic was used. The expression of other variables did not show any trends or differences between classes. Selection was supported by the recommendations of Thiel et al. (2009), which states that Mean is the most suitable for classification and that the best results were achieved by Mean.

Results were stored and visualised in Microsoft Excel. Analysis of statistics results is presented in chapter 5.2. The overall workflow diagram is illustrated in Appendix 1.

7.2 Result of analysis

The mean intensity values of single fields were collected from the images during the year 2016. There were 12 fields of maize, 10 fields of spring grains and 10 fields of winter grains. The values of backscatter intensity and their trend of evolution during the vegetation season was visualised in the graphs as you can see below in Fig. 11 and Fig. 18.

Figure 11: Seasonal backscatter in VH polarisation

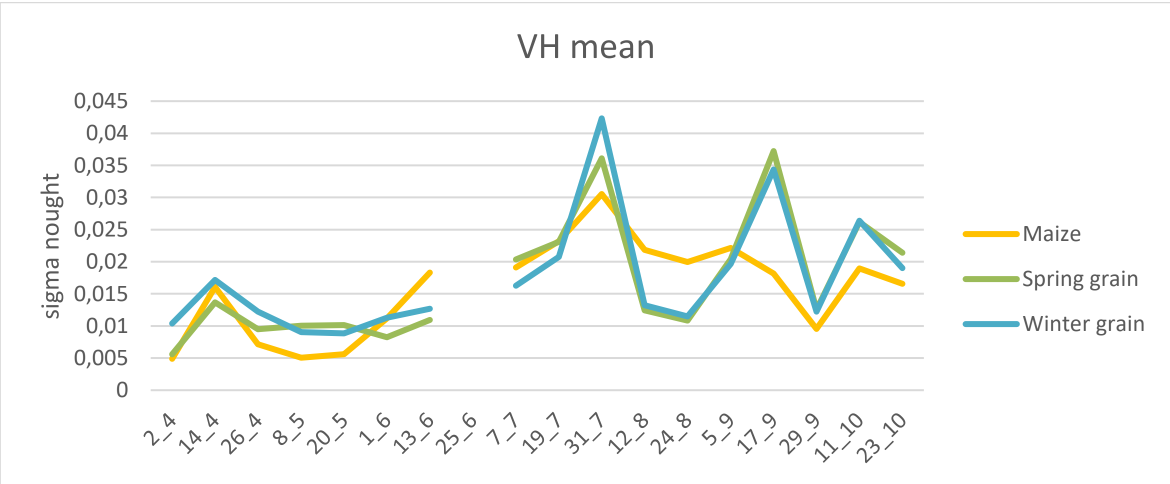

Source: Own production

In April 14, July 31 and September 5 there are significant increases in mean sigma nought values in VH polarization. Those peaks do not really express the real characteristics of fields. According to data collected by ČHMÚ (see Fig. 10 and Tables 4, 5) those measurements were affected by rainfalls. As was explained before, soil moisture increases backscatter. Beside of this anomaly we could observe the phenological phases of crop types. In general it could be seen that the values are really low, even comparing to VV polarization. From the graph there can be seen low values from April almost until beginning of June. In this period there are no double reflections that could depolarize the signal. Even though little higher values could be measured in fields of winter grains. As can be seen on the illustrative picture of growing cycle of winter wheat (Figure 13), at the end of March and beginning of April, plants are already growing. Even the length of 9 cm can affect the signal in C band. During the field observation the photo was taken that can illustrate the situation in early spring, when winter grains already start to grow and spring grains fields are still bare. Illustrative pictures are in the Figure 13 and 14.

Figure 12: Winter wheat growth stages

Source: Thomas (2015)

Figure 13: Winter grains field in April

Source: GISAT (2017)

Figure 14: Spring grains field in April

Source: GISAT (2017)

The spring grains fields start to express themselves little later in VH. As was expected, the maize is planted last. (Kowalski CH, 2017) Its VH reflection increases in June. The increase in June and July, is connected with growing of crops. Higher volume scattering is present. All types of crops have higher VH reflection. Illustrative pictures from field survey are in Fig 15, 16 and 17

Figure 15: Winter grains in June

Source: GISAT (2017)

Figure 16: Spring grains field in June

Source: GISAT (2017)

Figure 17: Maize field in June

Source: GISAT

The harvest of winter and spring cereals occurs mainly in July and beginning of August. The sharp drop in August means the harvest. It means that the harvest took place in between last day of July and August 12. Flat and dry surface does not cause much amount of depolarized backscatter. In the period of this drop the maize fields are still in ongoing maturation. The values are getting lower because of drying but there is still canopy backscatter. The harvesting of maize is carried out in late September which is visible on the decrease of VH values in September 29. The second drop is visible there. In September there is a peak and drop in values that are visible in winter and spring grains classes. Even the harvest was already done. According to meteorological data, there was precipitation on September 5. This fact again makes interpretation difficult. Beside of soil moisture effect, other reasons could be considered. In some cases, after the first crops are harvested, other crops are grown. Some farmers leave the field for grass to fertilize. In some cases it was directly confirmed by field survey. Last increase of backscatter in October represents ploughing that is done in all three crop types. After ploughing the ground is rough. And as was mentioned previously roughness increases backscattered energy.

Figure 18: Seasonal backscatter in VV polarization

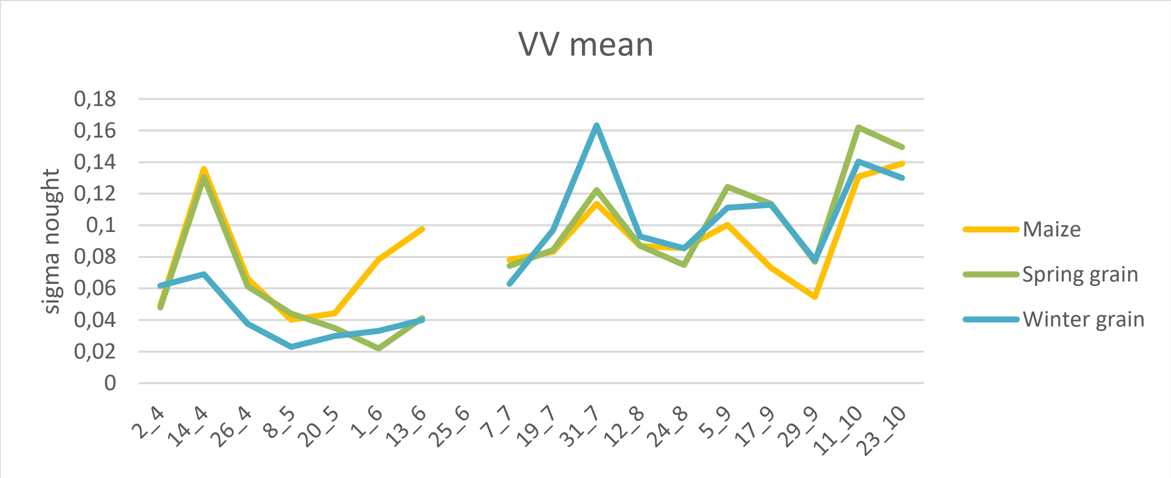

Source: Own production

The Fig. 19 shows phenological phases of selected crops in VV polarization. It could be seen that sigma nought values of VV polarization are higher than VH polarization. Almost by decimal point. In the graph there are the same peaks in the same dates that are influenced by rainfalls. VV band emits and receive vertical polarized signal. This signal represents single backscatters. In the spring months the signal react moreover only with soil. In the middle of April, winter grains differ from others. Winter cereals are the only growing in this period of time. That means that the crop depolarizes the signal and original vertical polarization is reflected less. However, this part of the data can not be used. Rainfall occurred on that day over selected territory. Described trend is visible until the period when spring grains and maize crops start to grow. Until that the values of VV are little lower.

It is difficult to comment values in June. The first two acquisitions are partly affected by rainfalls and the last one is missing. Despite that there is no significant increase of values that could signify that the fields are affected by rainfall. Spring and winter grains are already growing and could be up to 60 cm high in June. That means that the signal is depolarized by interaction with stems and its canopy. Trend of growing backscatter in VH values is observable in Fig.11. That means less of vertical backscatter from bare soil is measured. Higher VV backscatter from soil is seen at fields of maize, which is observable on the graph in Fig. 18. Maize starts it growing cycle later. But since there is possibility of rainfall effect, it can not be said with certainty. The reflectance of maize in VV could be higher because of higher interaction with soil. Reason for different backscatter could be caused by differences between canopy. Spring and winter grains has higher density of thin stems. (Mingquan J. et al., 2013) Maize has different stem from other two crops. The energy is reflected by single backscatter from bare soil but could be reflected by single backscatter from strong stem. That means that more of vertically polarized signal is measured by interaction with its stem. The peak in the end of July is also effect of rainfalls as was mentioned before. The harvest in August that was represented as decrease of VH values is not visible in VV polarisation. Single backscatter from bare land in August on spring and winter grains is present. In this phase, the soil is dry. Dry soil does not reflect radar signals that much and so the measured backscatter did not increase.

In September, there is a little increase of backscatter of VV in winter and spring grains fields. It is partly by rains and could be partly by early ploughing. The last decrease signify final cut off and drought. Maize and additional crops are harvested. During harvest is drought and dry soil reflects less energy. Also the area is bare and flat at that time. The backscatter energy is low. The final increase is caused by ploughing. Rough surface cause higher backscatter in all crop types. And it is also supported by precipitation in October 11.

8 Classification and accuracy assessment

8.1 Classification

In the first place it was needed to choose data that will enter the process of classification. It would be redundant to use all dataset. Based on the analysis and notes of the dates with highest differences, the images of VH polarization from August 24 and September 17 were chose. Also the VV polarisation image from June 13. Those can differ spring and winter cereals from maize. The spring from winter cereals are difficult to distinguish. The acquisition from April 2 in VH polarisation was used. According to analysis, these are the dates when the differences are measurable. The choice is in agreement with the theory of avoiding the use of images affected by rain. (Blaes, 2002)

When the acquisition dates were chose, the images were stacked into one file. The process was done in Envi 5.3. Function *Layer Stacking* was used. These single images were stacked in one image as individual bands. To simplify and refine the process of segmentation and classification, mask of agricultural area was used. The input raster was masked by layer of agricultural fields. Polygons that were reduced by 40 m at the borders were used. This theory was accepted from Blaes (2002)

The process of classification starts with segmentation. Individual segments responded to masked raster fields. Thanks to preview window appropriate values of Scale and Merge level were set to obtain compact segments that correspond to the raster dimension. In Figure 20 you can see the segments that correspond with masked raster. Segmentation algorithm *Edge* and merge algorithm *Full Lambda Schedule* was chose. Algorithm *Edge* divides the image by detecting edges. Sharp differences in intensity values create the segments. The *Scale level* values affect the selection. Higher the value, more objects divided with sharp edges. *Full Lambda Schedule* merges neighbouring segments with similar spectral and spatial characteristic. (Exelis VIS-a, 2017)

Scale level was set on the value 100 and *Merge level* on the value 100. It was intended to create segments corresponding to the masked area. For this reason, maximum values were selected.

Figure 19: Segmentation overview

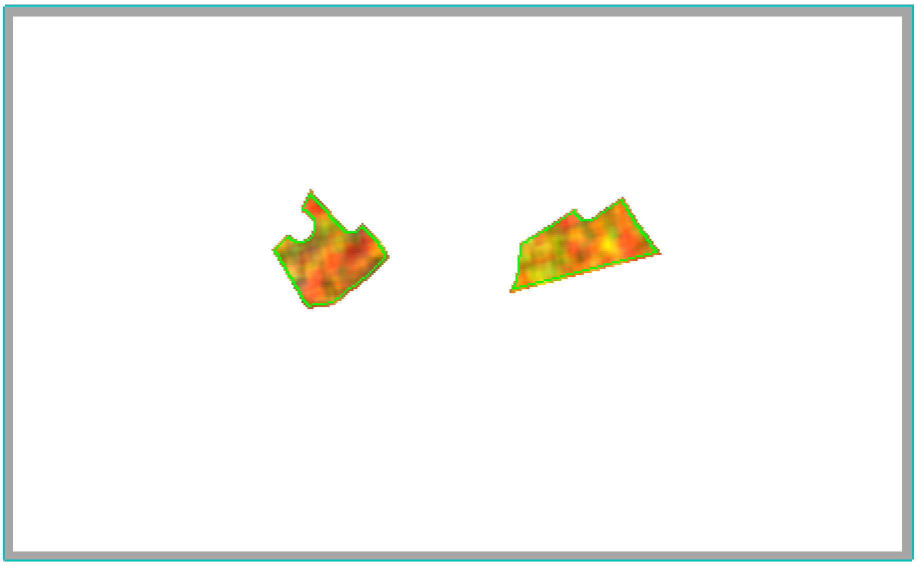

Source: Own production

Rule-based approach

The rules were created according to the results of multi-temporal analysis of mean values of VV and VH polarization. For individual classes different attributes were set. At first it was meant to separate spring and winter grains from maize. In the graph there are visible differences in June 13 in VV polarisation and especially in August 24 and September 17 in VH polarisation. To separate spring and winter grains the image from April 2 was used. In Tables 6, 7 and 8 there are used rules for this classification with which the best results were achieved. Threshold values were set as was optional, maize 0.3, spring grains and winter grains 0.4.

Table 6: Classification rules for Maize

	image	mean values
Maize	June 13 VV	0.0889 - 0.1187
	August 24 VH	0.0182 - 0.0243
	September 17 VH	0.0150 - 0.0194

Source: Own production

Table 7: Classification rules for Spring grains

	image	mean values
Spring grains	April 2 VH	0.0030 - 0.0080
	June 13 VV	0.0200 - 0.0600
	August 24 VH	0.0081 - 0.0139
	September 17 VH	0.0250 - 0.0350

Source: Own production

Table 8: Classification rules for Winter grains

	image	mean values
Winter grains	April 2 VH	0.0080 - 0.013
	June 13 VV	0.0300 - 0.0500
	August 24 VH	0.0081 - 0.0139
	September 17 VH	0.0260 - 0.0350

Source: Own production

8.2 Accuracy assessment

At the end of all classifications the part evaluations of results have to be presented. For classification evaluation was used the same software Envi 5.3. The function *Confusion Matrix Using Ground Truth ROI*s was used. The validation polygons were used as rois in this part.

Confusion matrix is a square array of numbers set out in columns and rows that express the number of sample units assigned to a particular category in one classification relative to the number of sample units assigned to a category in another classification. (Congalton et al., 1999) The columns of the matrix are the pixels of the class to which they belong. In rows there are pixels whose were classified in that class. The correctly classified pixels are located on the main diagonal of the matrix. Every other parts out of diagonal represent wrongly classified pixels. There are two categories of errors. Errors of commission is an error situation when pixels are wrongly classified. Errors of omission represent the pixels that belong to a class but were predicted to be in a different one. Other statistics that describe the results are Overall Accuracy which is a sum of correctly classified pixels divided by total number of pixels. (Exelis VIS-b, 2017) The Kappa coefficient compares the result of the classification with the classification resulting from the purely random process of classifying pixels. It is based on the assumption that even in a purely random classification, part of the pixels will be classified correctly. It can take values from zero to one. The value 1 means 100 % conformity and 0 represents no agreement. (Jensen, 2005) Other statistics are Producer's Accuracy and User's Accuracy. The difference between Producer's and User's Accuracy is that Producer's Accuracy is a ratio of correctly classified pixels and pixels from validation polygons. User's Accuracy is a probability that the classified pixel on the map represents the category on the ground. It is a ratio of correctly classified pixels and the sum of all pixels that were classified into the same class. (Exelis VIS-b, 2017)

Confusion matrix as a result of classification is in Table. 9. The overall accuracy reached 62 %. Although general and universal characteristic to determine success is the overall accuracy, it is more important and interesting to focus on the separate classes and their position due to diagonal of error matrix. (Congalton et al., 1999)

Best results were achieved in the class maize. Its producer's accuracy is 83,27 %. In the row of Maize there is visible that there is low percentage of pixels that actually belong to another classes. Only 3,02 % pixels from spring grains and 4,98 % from winter grains were committed into the class maize. The small amount confirms success in the maize classification. The commission error is 11,01 %. The omission error is also small. The number of pixels that were wrongly classified into other classes is relatively small. Omission error of maize is 16,73 % and the majority of this misclassification was into the class of spring grains (13,79 %).

Spring grains were not classified that precisely as maize. The producer's accuracy is only 59,23 %. The highest misclassification was between winter grains. Their mutual misclassification is clearly visible from the error matrix. Over 37 % of spring grains pixels were classified into winter grains. Winter grains make up most of the omission error of spring grains which is 40,77 % (see Table 10). There was not a significant number of pixels classified into the maize class, only 3,02 % as was already written. Commission error is higher. Almost 14 % of maize pixels were wrongly classified into the spring grains. In addition to omitted pixels from winter grains (46,14 %), the total commission error is 53,62 % (see Table 10).

The class of winter grains has the lowest producer accuracy. Only 48,88 % of pixels were classified correctly. Nearly the same portion of pixels were poorly classified into spring grains. More than 46 % of pixels were committed into the class spring grains. The amount of committed pixels in the maize class is low in comparison with spring grains. This confirms good mutual separability of classes maize and winter grains. On the other hand the separability between spring and winter grains is low.

User’s accuracy of maize is 88,99 %. That means that 88,99% of pixels that is classified as maize is actually maize on the ground. The user's accuracies of winter and spring grains are incomparably smaller. Class spring grains has only 46,38 % and class winter grains only 59,65 %. That means that only 46,38 % pixels of spring grains and 59,65 % pixels of winter grains in the map are in the same classes on the ground.

Kappa coefficient is a measure of how well the classification agrees with the reference data. The Kappa coefficient is 0,4285 (see Table 11). According to Cohen’s (1960) categorization the result can be interpreted as moderate agreement.

Table 9: Confusion matrix of Rule based classification

	Validation data				
	Classes	Maize	Spring grain	Winter grain	Total
Classified data	Maize	83,27 %	3,02 %	4,98 %	26,62 %
	Spring grain	13,79 %	59,23 %	46,14 %	41,15 %
	Winter grain	2,94 %	37,75 %	48,88 %	32,22 %
	Total	100 %	100 %	100 %	100 %

Source: Own production in Envi

Table 10: Commission and Omission Errors

Classes	Commission error [%]	Omission error [%]
Maize	11,01	16,73
Spring grain	53,62	40,77
Winter grain	40,35	51,12

Fig. 1: Own production in Envi

Table 11: Producer's and User's accuracy, Overall Accuracy and Kappa coefficient

Classes	Producer Accuracy [%]	User Accuracy [%]
Maize	83,27	88,99
Spring grain	59,23	46,38
Winter grain	48,88	59,65
Overall Accuracy	62,00	
Kappa coefficient	0,4285	

Fig. 2: Own production in Envi

9 Discussion

The classification results of maize are satisfactory. The maize class was separated from the spring grains and winter grains successfully. Producer's and user's accuracies of Maize achieved satisfactory results. More than 83 % of pixels were classified correctly. Multi-temporal analysis correctly revealed the best rules for its correct classification. June 13, August 24 and September 17 were chose as most suitable. The maize with its vegetation cycle is significantly different from the spring grains and winter grains. Its seasonal backscatter is thus easier to identify and then the efficient rules for its classification can be made.

Although the overall accuracy of classification may be seem successful in a more detailed view, we can find out that it is not. It is not possible to claim that the results of spring grains and winter grains were satisfactory. From the confusion matrix, mutual misclassification can be observed. Producer's accuracy of spring grains was 59,23 % and winter grains was only 48,88 %. The reason of this misclassification are similar backscatter statistics that were measured during the season. The classification rules could not separate these two classes with good results. Similar difficulties with classification of maize and cereals had Forkuor et al. (2014)

The reason for poor results can be caused by small sample of data. It is possible that the sample that was the basis of multi-temporal analysis was not representative for the whole dataset. The backscatter statistics did not show appropriate differences and for this reason also the classification rules of spring grains and winter grains were not representative. Another reason could be that the sample data had some anomaly which is not present in the rest of dataset. That could also lead to wrongly set rules and then misclassifications and errors. Or as Congalton et al. (1999) say, errors could be made by mistakes in reference data. Error matrices can be inadequate indicators of map error, because they are often confused by errors in the reference data.

The reason for unsatisfactory separation of spring grains and winter grains can be absence of images where the differences are measurable. It is possible that their phenological cycle is not that similar as presented in Fig. 12 and 19. There are images affected by rainfalls. The backscatter values in these images are affected by water. There is a possibility that the classes differ in those dates. However without images not affected by precipitation it can not be proven.

A solution that would eliminate errors and improve classification is to use a larger sample of ground truth data. A larger sample can better filter out anomalies and have a better match with the entire dataset. Differences between classes will be more observable. Another solution to improve the results is to obtain more imagery data. Especially those that are not affected by rainfalls. Sentinel-1 already produces images with 6 days period. It gives a higher probability that more appropriate images will be available. Higher chance that the classification rules will be more efficient.

In addition to usage of Intensity with dual polarization, there is another potential for improvement. The usage of phase. Moeremense and Dautrebandeho (1998) and Klenke and Hochschild (1999) suggest to use coherence for crops detection. Also usage of textural features as Schistad Solberg et al. (1997) and Pingxiang and Shenghui (2003) suggest.

10 Conclusion

The aim of the diploma thesis was to investigate the use of SAR C-band data in the field of agricultural crop detection. Evidence to meet this partial goal can be a comprehensive review of past research and a description of the C-band's dual polarization reflective properties. Basic SAR information was introduced. History and general characteristics were noted. Difficulties of acquisition and processing have been described. A new type of data and new processing software were introduced. SENTINEL-1 data and its specifics were investigated. New open source software SNAP, developed by ESA was used. Multi-temporal classification approach has been investigated and an analysis of selected crops with dual polarisation VV and VH has been carried out. Their backscatter properties were put into the context of phenological phases. The effect of moisture on reflectivity of radar radiation was confirmed by meteorological data. Thus confirming the importance of these data when working with radar data. Object based classification have been made on the basis of the findings, with the aim of confirming the distinctiveness of the crops. The combination that resulted in best accuracies consists from four images. April 2 (VH), June 13 (VV), August 24 (VH) and September 17 (VH). Satisfactory distinctiveness has been confirmed only for maize. Maize has achieved 83,27 % accuracy. Spring grains and winter grains have poor results and only achieved 59,23 % and 48,88 % accuracy. The reason for poor results was explained by excessive similarity of backscatter coefficient during the whole season. It was not possible to create rules that would differentiate these two classes satisfactorily.

The work confirmed SAR data in C-band as an appropriate source for agriculture observations. Although the results of the classification are satisfactory only partially, the work confirmed the potential of SAR C-band data in crop classification, which is worth to examine. In the future, it is advisable to extend the dataset of images to have higher chance to reveal differences between classes. It is advised to use phase component that can support the process of rulemaking and then achieve better classification results.

Bibliography

APIC (2017): Agrární poradenské a informační centrum. Available at: http://www.apic.cz/1028-sance-a-rizika-casneho-vysevu-kukurice.html

ARPA (2017): Agriculture and rural payments agency, Land Parcel Identification system, available at: https://secure2.gov.mt/mrra-pa/lpis?l=1

BLAES X. et al. (2002) Third International Symposium on Retrieval of Bio- and Geophysical Parameters from SAR Data for Land Applications, Sheffield, pp. 47-56

BRAUN A. (2017): STEP Forum, Sentinel-1 Intensity analysis, available at: http://forum.step.esa.int/t/sentinel-1-intensity-analysis/5043/4?u=kkop, (retrieved 2017-4-24)

CAMPBELL J. B. (1987): Introduction to Remote Sensing, Guilford, New York, p. 551

ČAPEK R. (1988): Dálkový průzkum Země, Ministerstvo školství ČSR, Praha, p. 244

CHMI (2017): Český Hydrometeorologický Ústav, Meteorologie a klimatologie, available at: http://portal.chmi.cz/pocasi

COHEN J. (1960): A coefficient of agreement for nominal scales, Educational and Psychological Masurement, vol. 20, no. 1, New York, pp. 37-46

CONGALTON R.G. et al. (1999): Assesin the Accuracy of Remotly Sensed Data: Principles and Practices, Lewis Publishers, Boca Raton, p. 137

COPERNICUS (2017): Application Domains, available at: http://copernicus.eu/main/application-domains

CRISP (2017): The Centre for Remote Imaging, Sensing and Processing, National Univeristy of Singapore, available at: https://crisp.nus.edu.sg/~research/tutorial/mw.htm

DEL FRATE F. et al. (2003): Crop Classification Using Multuconfiguration C-Band SAR Data, IEEE Transactions on Geosence and Remote Sensing, vol. 41, no. 7, pp. 1611 – 1618

EAGRI (2011): Zemědělství a změna klimatu, Ministerstvo zemědělství, Praha p. 28

ESA (1993): Use of ERS-1 SAR Data for agricultural, forestry and environmental applications in central-eastern Europe, Frascati, p. 136

ESA (2013): Sentinel-1 User Handbook, available at: https://sentinel.esa.int/documents/247904/685163/Sentinel-1_User_Handbook, p. 80

ESA (2015): Copernicus, available at: http://www.esa.int/Our_Activities/Observing_the_Earth/Copernicus (downloaded 17. 8. 2015)

ESA (2017): Radar course 2, available at: https://earth.esa.int/web/guest/missions/esa-operational-eo-missions/ers/instruments/sar/applications/radar-courses/content-2/-/asset_publisher/qIBc6NYRXfnG/content/radar-course-2-synthetic-aperture-radar

ESA-b (2017): Reference Mission Orbit, available at: http://seom.esa.int/insarap/files/INSARAP-2014_Results_from_Sentinel-1A_Commissioning_Phase_DGeudtner.pdf

ESA-c (2017): SAR Instrument available at: https://sentinel.esa.int/web/sentinel/technical-guides/sentinel-1-sar/sar-instrument

ESA-d (2017): https://sentinel.esa.int/web/sentinel/user-guides/sentinel-1-sar/data-formats/safe-specification

ESA-e (2017): News, Aral Sea, available at: https://earth.esa.int/web/guest/-/aral-sea-6368

EXELIS VIS-a (2017): Rule based classification, available at: http://www.exelisvis.fr/docs/rule_based_classification.html

EXELIS VIS-b (2017): Calculate Confusion Matrices, available at: https://www.harrisgeospatial.com/docs/CalculatingConfusionMatrices.html

FARR G. T. (1993): Guide to Magellan Image Interpretation, chapter 5, Radar Interactions With Geologic Surfaces, JPL Publications, pp. 45-56

FERRAZZOLI P. (2001): SAR For Agriculture Advances, Problems and Prospects, Third International Symposium on Retrieval of Bio- and Geophysical Parameters from SAR Data for Land Applications, Sheffield, pp. 47-56

FORKUOR G. et al. (2014): Integration of Optical and Synthetic Aperture Radar Imagery for Improving Crop Mapping in Northwestern Benin, West Africa, Remote Sensing, vol 6. pp. 6473 – 6499

GAGNON L., JOUAN A. (1997): Speckle Filtering of SAR Images – A Comprarative Study Between Complex-Wavelet-Based and Standard Filters, Département de R&D, Montréal, Canada, p. 12

GRANDONI D. (2013): Advantages and limitations of using satellite images for flood mapping, Workshop on the use of the Copernicus Emergency Service for Floods, Brussels, available at: http://www.copernicus.eu/sites/default/files/documents/User_uptake/Emergency_Events/Athens/03_Session_01_AdvantageAndLimitationsOfUsingSatelliteImagery.pdf

HALOUNOVÁ L. (2004): Klasifikace černobílých leteckých snímků a radarových dat. Habilitační práce. Katedra mapování a kartografie FSv ČVUT, Praha, 143 p

HUANG Y., van GENDEREN J.L. (1996): International Archive of Photogrammetry and Remote Sensing. Vol. XXXI, Part B2, Vienna, pp. 164-169.

JENSEN J. (2000): Remote sensing of the environment: an earth resource perspective, Pearson Prentice-Hall Upper Saddle River, p. 608

JENSEN, J. (2005): Introductory Digital Image Processing: A remote Sensing Perspective. Pearson Prentice Hall, Upper Saddle River, p. 526

JOHANNESSEN J. A. et al. (2013): SAR Instrument Principles and Processing, 3rd ESA Advanced Training on Ocean Remote Sensing, Cork, available at: https://earth.esa.int/documents/10174/950595/01_Wednesday_OCT2013_SAR_principles.pdf

KIM J. et al. (2012): Comparing Image Classification Methods: K-Nearest Neighbor and Support Vector Machines, 6th WSEAS international conference on Computer Engineering and Applications, Cambridge, p. 6

KLENKE M., HOCHSCHILD V. (1999): Improving SAR Intensity-Based Land Cover Classification Results by the Use of Interferometric Coherence Information and GIS-Analysis , Proceedings of the IGARSS'99, pp. 2108 – 2110

KOLÁŘ J. (2008): Radarová obrazová data a jejich využití. Česká komická kancelář. Praha, p. 55

KOWALSKI CH. (2017): Corn Planting and Harvest seasons, The balance, available at: https://www.thebalance.com/corn-planting-and-harvest-seasons-809309

LAGERGOUSE (2017): Agro Morava, Doporučené výsevky zemědělských plodin, available at: http://www.lagerhaus.cz/gallery/lagerhaus_osiva.pdf

LEE J. S., POTTIER E. (2009): Polarimetric radar imaging from basics to applications. CRC Press, Florida, p. 398

LIU D., XIA F. (2010): Assessing object-based classification, advantages and limitations, Remote Sensing Letters vol. 1 no. 4 pp. 187-194

MANSOURPOUR M. et al.(2006): Effects and performance of speckle noise reduction filters on active radar and sar images, Tehran, Alberta, p. 6

MINGQUAN J. et al. (2013) Multitemporal radar backscattering measurement of wheat fields using multifrequency (L, S, C, and X) and full-polarization, Radio Science, vol. 48, pp. 471–481

MOEREMANS B., DAUTREBANDE S. (1998): Use of ERS SAR interferometric coherence and PRI images to evaluate crop height and soil moisture and to identify crops, Remote Sensing for Agriculture, Ecosystems, and Hydrology, vol. 9, p. 10.

MOURATIDIS Antonios - personal conversation (external collaborator at Department of Applied Geoinformatics and Cartography, Albertov 6, Praha 2), 22. 2. 2017

NASA (1987): SAR (Synthetic Aperture Radar). Earth observing system, vol. IIf, Instrument panel report, Greenbelt, Maryland

NEST (2017): Next ESA SAR Toolbox Overview, Orthorectification, available at: http://corp.array.ca/nest-web/help/operators/RangeDopplerGeocodingOp.html
(downloaded 14.6.2017)

NEST (2017): Orthorectification available at: http://corp.array.ca/nest-web/help/operators/RangeDopplerGeocodingOp.html

NRCAN-a (2017): Fundamentals of Remote Sensing, available at: http://www.nrcan.gc.ca/node/14639

NRCAN-b (2017): Viewing geometry and spatial resolution available at: http://www.nrcan.gc.ca/earth-sciences/geomatics/satellite-imagery-air-photos/satellite-imagery-products/educational-resources/934

OLLEGGINI L. (2008): Rule-based crop area classification using multi-temporal, multi-source data, Zurich, p. 99.

OLOFSSON P., et al. (2013): Good Practices for Assessing Accuracy and Estimating Area of Land Change, Remote Sensing of Environment, p. 57

PARKER W. V. (2012): Discover the Benefits of Radar imaging, Earth Imaging Journal available at: eijournal.com

PINGXIANG L., SHENGHUI F (2003): SAR Image Classification Based on Its Texture Features, Geo-spatial Information Science, volume 6, issue 3, pp. 16-19

Radar Basics (2017): Synthetic Aperture Radar, available at: http://www.radartutorial.eu/20.airborne/ab07.en.html

SAICH P., BORGEAUD M. (2000): Interpreting ERS SAR Signatures of Agricultural Crops in Flevoland, 1993-1996, IEEE Transaction on Geoscience and Remote sensing, vol. 38., no. 2, pp.651-657

SARTI F. (2009): ESA Earth Observation Programmes, Reminder about SAR, Bucharest, p. 165

SATALINO G. et al. (2014): C-Band SAR Data for Mapping Crops Dominated by Surface or Volume Scattering, Geoscience and Remote Sensing, vol. 11 no. 2. Pp. 384-387

SCHISTAD SOLBERG A. H et al. (1997): Texture Fusion and Feature Selection Applied to SAR Imagery, Transactions on Geoscience and Remote Sensing, vol. 35, no. 2, pp. 475-479

SCHMULLIUS C., NITHACK J. (1995): Crop Monitoring With Multi-Temporal Airborne DLR E-SAR Images, Geoscience and Remote Sensing Symposium, Proceedings of the IGARSS'95, pp. 719 – 721

SKRIVER H. (2011): Crop Classification Using Short-Revisit Multitemporal SAR Data, IEEE Journal of Selected Topics In Applied Earth Observations And Remote Sensing, vol. 4, no. 2, pp. 423-430

SKRIVER H. (2012): Crop Classification by Multitemporal C- and L- Band Single- and Dual- Polarization and Fully Polarimetric SAR, IEEE Transaction on Geoscience and Remote sensing, vol. 50., no. 6. pp. 2138 – 2149

SKRIVER H. et kol. (1999): Crop Classification by Polarimetric SAR, Geoscience and Remote Sensing Symposium, Proceedings of the IGARSS'99, pp. 2333 – 2335

SlideShare (2010): Object Based Image Analysis, www.slideshare.net/kabiruddin/object-based-classification

TAVAKKOLI SABOUR S.M. et al. (2012): Mapping of agricultural activities using multi-temporal ASAR Envisat data, Institute of Photogrammetry and GeoInformation Leibniz University of Hannover, p. 7

THIEL C. a kol. (2009): Analysis of multi-temporal land observation at C-band. Geoscience and Remote Sensing Symposium, IEEE International, IGARSS 2009, č. 3, pp. 318–321.

THOMAS S. (2015): When are Soviet Fields In-Season or Out-of-Season in Crossfire?, Balagan, available at: http://balagan.info/when-are-soviet-fields-in-season-or-out-of-season-in-crossfire

TSO, B., MATHER, P. M. (1999): Crop discrimination using multi-temporal SAR imagery. International Journal of Remote Sensing, vol. 20, n. 12, pp. 2443–2460

USGS (2015): Shuttle Radar Topography Mission, available at: https://lta.cr.usgs.gov/SRTM1Arc (downloaded 31.5. 2017)

VECI L. (2016): SAR Basics Tutorial, ESA, Array Systems Computing Inc., p. 19

LIST OF APPENDICES

Appendix 1: Workflow diagram